Evaluation of diffusion parameters and phase formation between tungsten films and glassy carbon

A.J. Innocent[a],*, T.T. Hlatshwayo[a], E.G. Njoroge[a], T.P. Ntsoane[b], M. Madhuku[c], E.O. Ejeh[a], M. Mlambo[a], M.Y.A. Ismail[a], C.C. Theron[a], J.B. Malherbe[a]

[a]Department of Physics, University of Pretoria, Pretoria, 0002, South Africa
[b]South African Nuclear Energy Corporation, South Africa
[c]iThemba Laboratory for Accelerator-Based Sciences (iThemba LABS), Private Bag 11, Wits, 2050, Johannesburg, South Africa

*Corresponding author. joseph.innocent@up.ac.za

Highlights

- Thin films of tungsten (W) were deposited on glassy carbon (C) substrates.
- The as-deposited samples were annealed isothermally under vacuum at temperatures ranging from 673 K to 1273 K.
- The structural changes due to thermal annealing were monitored by RBS and GIXRD.
- The GIXRD analysis showed that carbide formation was first observed at annealing temperature of 1173 K.
- The W/C system was stable under heat treatments below 1073 K.

Abstract

Thin films of tungsten (W) were deposited on glassy carbon (C) substrates using a magnetron sputtering system. The as-deposited samples were annealed isothermally under vacuum at temperatures ranging from 673 to 1273 K. The structural changes due to thermal annealing were monitored by Rutherford backscattering spectrometry (RBS) and grazing incidence X-ray diffraction (GIXRD). RUMP software was used to simulate the RBS spectra. The thickness of W thin films deposited, atomic composition of deposited layer and the intermixed layer growth were deduced from the RUMP simulation results. The GIXRD analysis showed that carbide formation was first observed at annealing temperature of 1173 K. The kinetics of the solid-state interaction was found to be diffusion controlled at the interface between W and C. The activation energy for the diffusion of C in W was estimated as 2.23 eV. The XRD results showed that the average crystallite size of the as-deposited W film was 9.77 nm. It increased with annealing temperature up to 18.05 nm at 1173 K. The first carbide phase observed was W_2C in the sample annealed at 1173 K, while WC was the dominant carbide phase at 1273 K. The stability of W/C system under heat treatments below 1073 K suggests that this system has a promising application for long-term structural integrity of dry cask storage devices.

Keywords: Glassy carbon; Tungsten; Annealing; Carbide; RBS; XRD

1. Introduction

Nuclear energy is one of the major contributors to the world energy resources but the task of storage and containment of nuclear waste has been a major scientific challenge to the growth and acceptability of this form of energy. These problems have adversely affected its acceptability by most members of the general public largely due to safety concerns. Currently, glass materials are being used for encapsulation of nuclear waste in solid form [1]. This waste is then stored in dry cask storage containers which are meant to be temporary until they are transferred to permanent geological sites. Demand for dry casks with longer service lifespan beyond 60 years [2] is expected to be on the increase in the near future due to dearth of permanent repositories. Currently, dry cask storage devices are made from materials such as stainless steel, cast iron and concrete. The problems with these materials are their susceptibility to corrosion and chemical attacks. A leakage of radiation as a result of defects caused by corrosion can pose serious threats to mankind and the environment. Hence, the need to research on new materials for extended service life of dry casks for nuclear waste storage. The maximum temperature of the spent nuclear fuel does not exceed 673 K [3]. This temperature decreases to about 473 K [4] after wet storage for few years, before being transferred to the dry cask storage device.

Carbon exists in many allotropic forms. In its natural form, carbon exists as amorphous carbon, graphite and diamond. It also exists in synthetic form as glassy carbon (C), fullerene, graphene, carbon nanotube and more recently as carbyne which is believed to be the strongest material in the world [5]. Carbon is unique because a change in its local bonding can give rise to the above-mentioned diverse materials [6]. These materials have a remarkable range of mechanical, electronic, and electrochemical properties and many possible applications. The ability of carbon to exhibit diverse properties originates from the flexibility to form sp^1, sp^2, and sp^3-hybridized bonds [7]. Glassy carbon is a synthetic form of carbon formed by pyrolysis of organic resins at elevated temperatures [8,9]. Glassy carbon exhibits a combination of glassy and ceramic properties with those of graphitic materials. It has high thermal stability and does not transform into graphite even at high temperatures up to 3273 K [10,11]. Glassy carbon possesses physical, chemical and mechanical properties which make it very promising for technological applications [12]. These properties include moderate hardness, resistance to corrosion and wear, high chemical inertness [13], impermeability to gases and liquids [14]. Other properties are high temperature stability, high thermal conductivity, good resistance to thermal shock and low coefficient of thermal expansion [15]. These properties make glassy carbon more useful for many industrial applications, such as vacuum evaporation sources, radiation containment, zone-refinement crucibles and encapsulation of spent nuclear fuel.

Tungsten is a heavy metallic element, a member of the third series of transition metals. Tungsten has the highest melting point of all metals, and at temperatures over 1923 K has the highest tensile strength [16]. It has good chemical, physical and mechanical properties; such as high thermal conductivity, irradiation resistance, exceptional corrosion and abrasion resistance. W also exhibits a low sputter rate and good thermal conductivity [17]. Due to these properties of W, it can serve two main applications in the nuclear waste storage system. First, being an element with high atomic number with massive nucleus, it can act as a shield component due to its ability to block gamma rays which low atomic number elements such as carbon cannot contain. Secondly, it is expected to provide structural enhancement due to its high mechanical strength. The W being a heavy metal is used for many applications, where the high specific weight of the material plays an important role. It is used as important components for X-ray and radiation shielding [18]. Typical examples of such shields are containers for radioactive materials and liquids, shielding construction parts in tomographic scanners, radiation therapy instruments, and containers and shielding for oil prospecting using radioactive sources [18].

The properties of glassy carbon enumerated above have drawn the attention of many researchers to study its performance improvement by ion implantation. Notable studies on ion species implanted in glassy carbon include Co [19], Cd [11], In [12] and Cs [20]. The results of these studies showed that the diffusion patterns of the implanted ions were not into the bulk, but rather towards the surface of the glassy carbon damaged by ion implantation. These observations suggested that glassy carbon was stable in radiation environment. Our literature search showed that phase formation as well as diffusion between tungsten and glassy carbon has not been studied. It is therefore, pertinent to investigate how W and glassy carbon interact under heat treatment. This will help to model these materials behavior under the influence of decay heat of radioactive nuclear waste. The knowledge from this study is important for developing new technology that will mitigate the challenge of nuclear waste management. The properties of these two materials highlighted above, could be explored in nuclear technology, especially in the dry cask component for radiation containment. The service lifetime of the iron-based canister can be improved by electrolytic treatment of its outer surface with layers of glassy carbon and tungsten. This will ensure sufficient protection against extended long term corrosion and chemical attacks.

2. Experimental procedure

Rectangular glassy carbon strips with dimensions of 50 mm X 10 mm X 2 mm were obtained from Hochtemperatur-Werkstoffe GmbH, in Germany. The Sigradur© G glassy carbon grade has a density of 1.42 gcm^{-3}, flexural strength of 260 MPa, compressive strength of 480 MPa, Young's modulus of 35 GPa, thermal conductivity of 6.3 $Wm^{-1}K^{-1}$ and maximum service temperature up to 3273 K [21]. The glassy carbon strips were cut into smaller sizes of 5 mm X 10 mm X 2 mm. Then W films were deposited on the glassy carbon substrates by physical vapour deposition. The MDX magnetron sputtering system made by Advanced energy industries, Inc [22]. was employed for sputtering tungsten films onto the glassy carbon substrates. The glassy carbon substrates were first mounted on a cleaned circular sample holder with a diameter of 10 cm, which was then mounted in the chamber of the magnetron sputtering system. The distance between the substrate and tungsten target was approximately 20 cm. The tungsten target is rectangular in shape with dimensions of 210 mm X 105 mm X 10 mm. The chamber pressure was first pumped down to 1 10^{-4} Pa and argon gas was introduced into the chamber with its pressure adjusted to 3 Pa giving rise to gaseous plasma in the chamber when the magnetron was switched on. The target was etched by Ar plasma for 5 min to ensure that any contaminant on its surface was removed before the actual sputtering process was carried out at room temperature. The sputtering parameters were carefully optimized after several attempts to ensure good adhesion between the W films and glassy carbon substrates. Films adhesion in both as-deposited and annealed samples was monitored by low magnification scanning electron microscopy. The optimized working gas pressure and sputtering power were 0.4 Pa and 145 W, respectively. The power density applied to the sputtering target was 0.66 Wcm^{-2}. Estimated average deposition rate of ~16 $nm{\cdot}min^{-1}$ was obtained for W films sputtered on the glassy carbon substrates.

The as-deposited tungsten-glassy carbon couples were annealed in a vacuum tube furnace annealing system with low pressure in the order of 1 X 10^{-5} Pa. Series of isothermal annealing were performed at temperatures ranging from 673 to 1273 K with a step interval of 373 K for various annealing duration of 30, 60, 90, 120, 180 and 1440 min. The as-deposited and annealed samples were analysed using the Rutherford backscattering spectrometry (RBS) system with the same analysis parameters given in Ref. [23] and the acquired spectra were simulated using RUMP code. The thickness of W layer deposited, elemental composition as well as information indicative of atomic intermixing across the interface of the diffusion couples were extracted from the RBS-RUMP simulated results.

In the conventional Bragg-Brentano configuration, the path travelled by the X-ray beam in thin films is too short for a typical Bragg angles to deliver X-ray reflections of sufficient peak-to-noise ratio [24], hence only negligible structural information is obtainable with this measurement configuration. This problem was circumvented in this study by employing the grazing incidence X-ray diffraction (GIXRD) configuration (shown in Fig. 1).

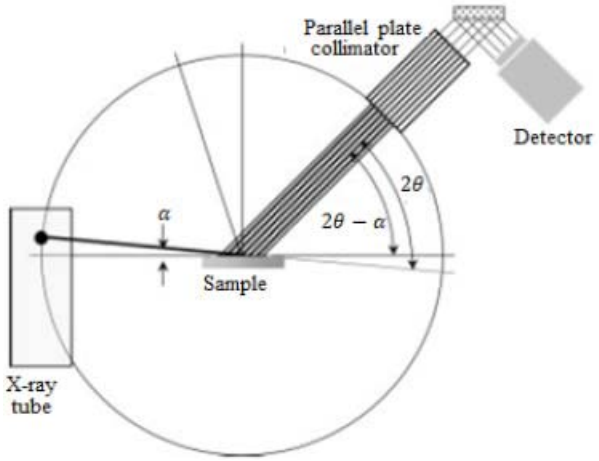

Fig. 1. The grazing incidence configuration. Adapted from Ref. [24].

With this configuration, the X-ray hits the W films at very low incidence angle of α = 1°. This arrangement helps to increase the path travelled by the X-ray beam in the W films before it eventually entered the glassy carbon substrates. This GIXRD configuration was used to measure all the samples using a Bruker-AXS diffractometer, with a Cu (K α) radiation source of wavelength 1.5406 *Å*, at 2-theta angle with a step size of 0.04°. The diffraction patterns were collected by a detector rotated on a goniometer from 15° to 100°. The samples were analysed by grazing incidence XRD in order to ensure that a high concentration of the radiation beam was on the deposited W films to ensure that sufficient structural information of the W films were acquired.

3. Results and discussion

3.1. RBS analysis

The RBS/RUMP simulated spectrum of the as-deposited sample is shown in Fig. 2. The red line denotes the simulated spectrum while the black one is the experimental RBS spectrum. The scattering events from W and glassy carbon (C) are clearly separated in energy. The W signal appeared at 1.47 MeV while the C signal appeared at a lower energy 0.40 MeV. The latter was due to both scattering kinetics and the energy loss of the backscattered He^+ ions, during their inward and outward paths.

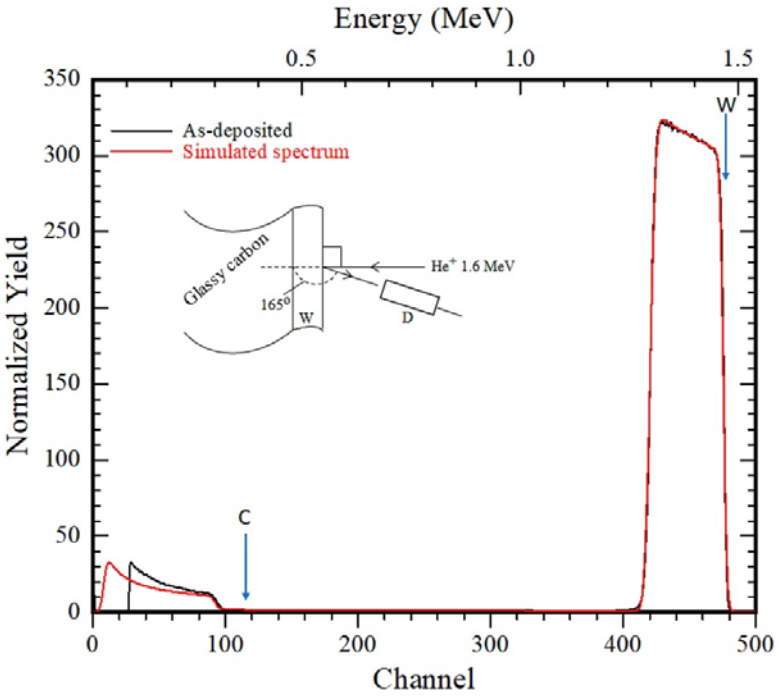

Fig. 2. The RBS spectrum of as-deposited sample (black) and RUMP simulated spectrum (red). Included in the figure is the experimental geometry.

The arrows at channel numbers 473 and 115 indicate the surface positions of W and C, respectively. If the C were present at the surface with W film, its signal would have appeared at the higher energy edge, indicated by the arrow in Fig. 2. The simulated spectrum overlaps the RBS measured spectrum very well, especially in the region of the tungsten signal, where the simulated and measured spectra are difficult to distinguish from each other. But at the lower energy channel of the C peak, it is difficult to achieve a good fit. This fitting problem at the low energy tail of the RBS is typical of this analytical method. Wang and Jacob [25], attributed this problem to the increasing background as a result of multiple scattering [26] from the overlaying W films, which is not quantitatively reproduced in the RUMP simulation program. Multiple scattering caused the traversing ions to possess reduced energy. This in turn produced a high scattering cross section, which resulted in high yields at the low energy tail. The effect of multiple scattering is common with layers of heavy elements and increases with layer thickness. The thickness of W film deposited on the C substrate was estimated as 726.8 X 10^{15} atcm^{-2} (i.e.~ 115.2 nm), bulk density was assumed for the W thin films.

The RUMP simulations of all the RBS spectra were also carried out to investigate the atomic intermixing between the W and C atoms for all the samples annealed at temperatures of 673–1273 K. The fit obtained from the as-deposited sample was coherently maintained in the simulations of the annealed samples. The simulated results for samples annealed isothermally from 673 to 973 K for annealing duration up to 1440 min showed that there was no sign of intermixing of atoms between the two materials in this temperature range. Their simulated spectra (not shown here) were similar to that of the as-deposited sample presented in Fig. 2.

Intermixing of W and C atoms was observed at 1073 K and increased progressively with annealing temperature and duration as presented in Fig. 3. This result was a little departure from our earlier finding [23] where the intermixing of W and C atoms appeared to have started at 973 K. This discrepancy can be attributed to the effect of difference in film thickness. The W

films used in the present study were thicker than the previous ones, which had a thickness of 62 nm. Jehn et al. [27], also observed similar results in their work on the reaction between amorphous carbon and tungsten. They reported that diffusion involving thinner films occurred at a lower temperature compared to thicker materials. Hugon et al. [28] observed that crystallite sizes were larger in thicker films compared to those in thinner ones. This implies that there is more accumulation of grain boundary in thinner films, which could aid atomic intermixing or diffusion at lower temperatures. Thin films are characterized by small grain sizes, which in turn give rise to more grain boundaries. The later act as pathways for diffusion in thin films even at low temperatures. For example, at an annealing temperature as low as 623 K, Lamble, et al. [29] reported that ditungsten carbide (W_2C) formed at the interface of C/W multilayer films. The C/W film thicknesses were 1.8 nm and 6.5 nm, respectively.

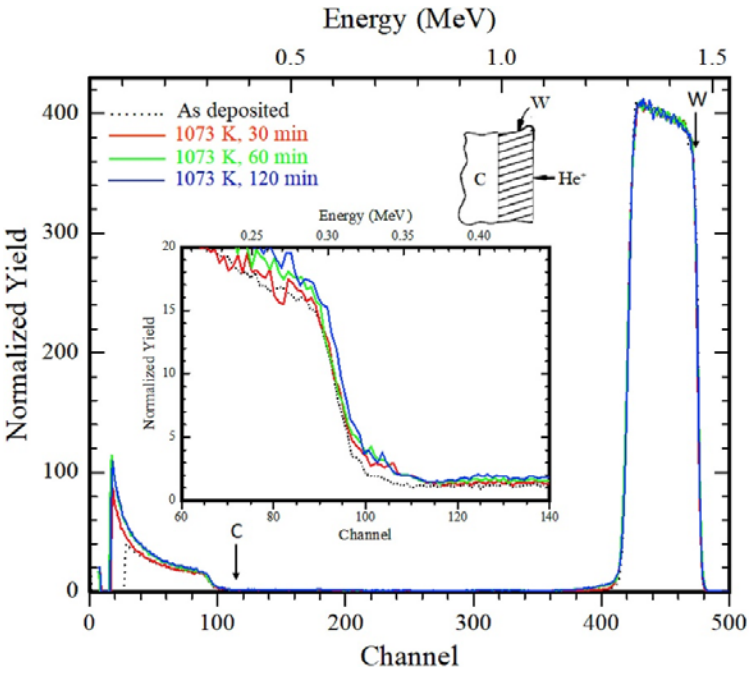

Fig. 3. The superposition of RBS spectra of as-deposited and the samples annealed at 1073 K for different annealing duration as indicated on the figure. Shown in the inset is evidence of atomic intermixing between W and C.

The simulated result of the sample annealed at 1073 K for 30 min, showed that there was an intermixed layer of thickness 6.32 X 10^{15} atcm^{-2}. In the sample annealed at 1073 K for 60 min, the thickness of intermixed layer was 8.64 X 10^{15} at cm^{-2} (simulated spectra not shown here). At 1073 K for 120 min, the simulated result showed that the intermixed layer widened to 13.96 X 10^{15} at cm^{-2}. In Fig. 3, the RBS spectra at 1073 K showed only small variation in the lower region of the W signal. This was an indication that, the annealed temperature was not high enough to trigger a substantial interface mixing, which could lead to phase formation in the diffusion couple. This is also evident in the height of the W signals for the annealed samples being the same with that of the as-deposited sample.

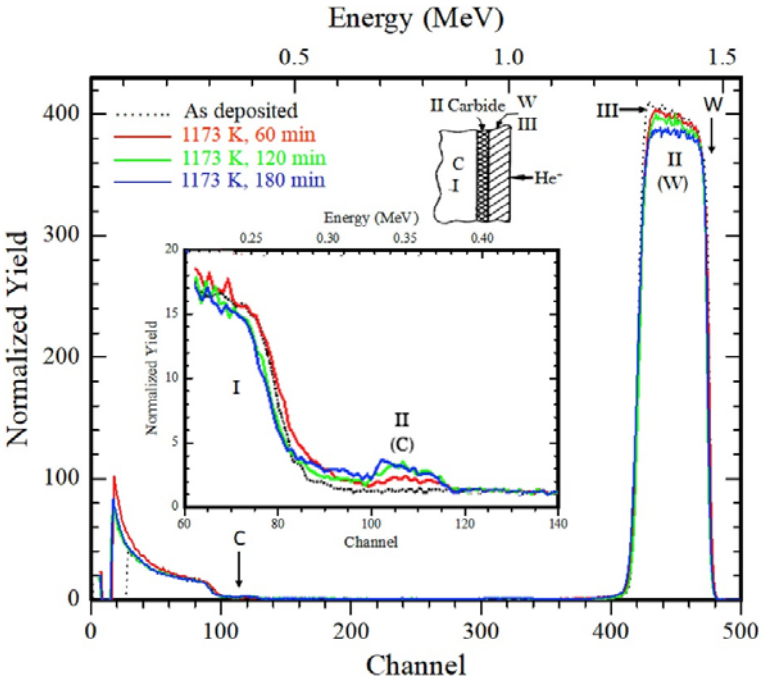

Fig. 4. The superposition of RBS spectra of as-deposited and the samples annealed at 1173 K for different annealing duration as indicated on the figure. The decrease in the W signal (II–W) and increase in the plateaus on the C signal (II–C) of the annealed samples correspond to the formation of the carbide phase. Shown in the inset is the reacted C (II–C) in the carbide phase.

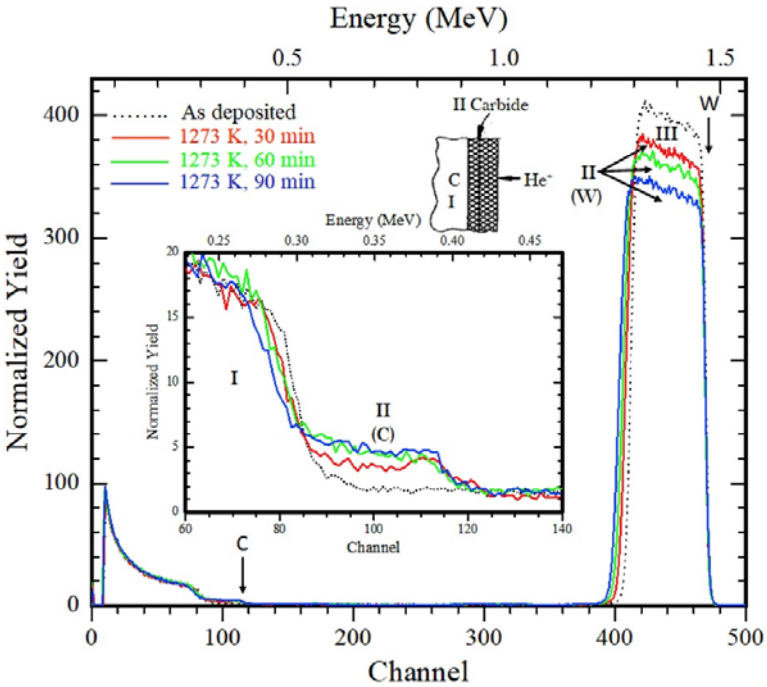

Fig. 5. The superposition of RBS spectra of as-deposited and the samples annealed at 1273 K, for different annealing duration as indicated on the figure. The decrease in the W signal (II–W) and increase in the plateaus on the C signal (II–C) of the annealed samples correspond to the formation of the carbide phase. Shown in the inset is the reacted C (II–C) in the carbide phase.

In Fig. 4, the spectra of the samples annealed at 1173 K for 60 min, 120 min and 180 min showed the presence of plateaus at the high energy edge of the C signal (region II in the inset). The appearance of these plateaus is an indication of carbide phase formation [30]. In Fig. 4, Fig. 5, regions II (C) and II (W) represent the reacted glassy carbon and tungsten atoms in the carbide phase, respectively.

On the other hand, the regions marked as I and III, correspond to unreacted glassy carbon and tungsten atoms, respectively. The simulated spectra of these samples showed an increase in the interaction between W and C atoms. This suggested carbide phase formation, however, it was difficult to predict the type of carbide phase based on the stoichiometry of W and C atoms obtained. Positive identification of phase is possible only with XRD. The thickness of the intermixed layers obtained at this annealed temperature are presented in Table 1.

Table 1. Intermixed layer growth with annealing temperature and duration.

Annealing temperature (K)	Annealing duration (min)	Intermixed layer thickness (10^{15} at·cm^{-2})
1073.0	30.0	6.3
	60.0	8.6
	120.0	13.9
1173.0	60.0	189.6
	120.0	216.8
	180.0	236.8
1273.0	30.0	282.3
	60.0	512.7
	90.0	267.7

Shown in Fig. 5 are the spectra of the samples annealed at 1273 K. After annealing at 1273 K for 30 min, a plateau developed on the high C edge [region II (C). The C signal of the carbide phase in this region extends to an energy corresponding to the presence of C at the sample surface.

It can be observed in Fig. 5 that the plateaus in region II (C) increased in height with increase in the annealing duration. The sample annealed at 1273 K for 90 min has the highest plateau. As these plateaus grow in response to the high temperature annealing duration, the W signals increased in width and reduced in height [region II (W)]. The W signals widen in width because C atoms which diffused from the glassy carbon substrate into W layer made those layers thicker. The C atoms in the W layer also lowered the concentration of the W in these layers, which resulted in the decrease of the W signal. As will be discussed below and will also be seen from the XRD results, the diffused C atoms also reacted with tungsten atoms to form carbide phase. The absence of a shoulder at the W back edges, suggested that C is the dominant diffusing species in this W/glassy carbon system. The plateaus in the intermixed region (II(C)) are flat shaped. This indicates the presence of constant composition of the carbide phase formed at these high temperatures.

The simulation results for the sample annealed at 1273 K for 30 min showed that the elemental composition was 65 at.% W - 35 at.% C. The ratio of W to C composition is approximately 2

which suggested the presence of ditungsten carbide (W_2C). Furthermore, the simulation results at 1273 K for 60 min and 90 min are essentially the same in terms of the elemental composition. The samples annealed at 1273 K for 60 min and 90 min have composition of 50 at. % W - 50 at.% C. The atomic composition for samples annealed at 1273 K for 60 min and 90 min showed that the tungsten monocarbide (WC) phase was formed at these extended annealing durations. The resulting intermixed layer thicknesses for samples annealed at 1073, 1173 and 1273 K are tabulated in Table 1. The intermixed layer of W and C associated with the high temperature annealing increased with both annealing temperature and duration.

From Fig. 4, Fig. 5, the RBS results of the annealed samples at 1173 K and above, clearly showed that the C atoms diffused into W layer. There is a large difference in the atomic radii of these materials. The atomic radius of carbon is 0.071 nm while tungsten has atomic radius of 0.137 nm [31]. This implies that the atomic size of tungsten is almost twice that of carbon. The diffusion of carbon in tungsten and its carbides proceeds via interstitial mechanism in addition to grain boundaries diffusion [18]. Elements with small atomic size such as carbon, nitrogen and oxygen usually undergo interstitial diffusion in tungsten.

3.2. Evaluation of diffusion parameters

The growth of the intermixed layer thickness (x) with annealing time (t) is often governed by the relation [32,33]:

$$x = kt^{1/2} \tag{1}$$

where k denotes the rate constant. Using the data in Table 1, the plots of x versus $t^{1/2}$ for the temperatures 1073, 1173 and 1273 K, gave straight line graphs [Fig. 6 (a-c)]. Also shown in the plots are error bars estimated from uncertainties associated with the simulations of the intermixed layer thicknesses.

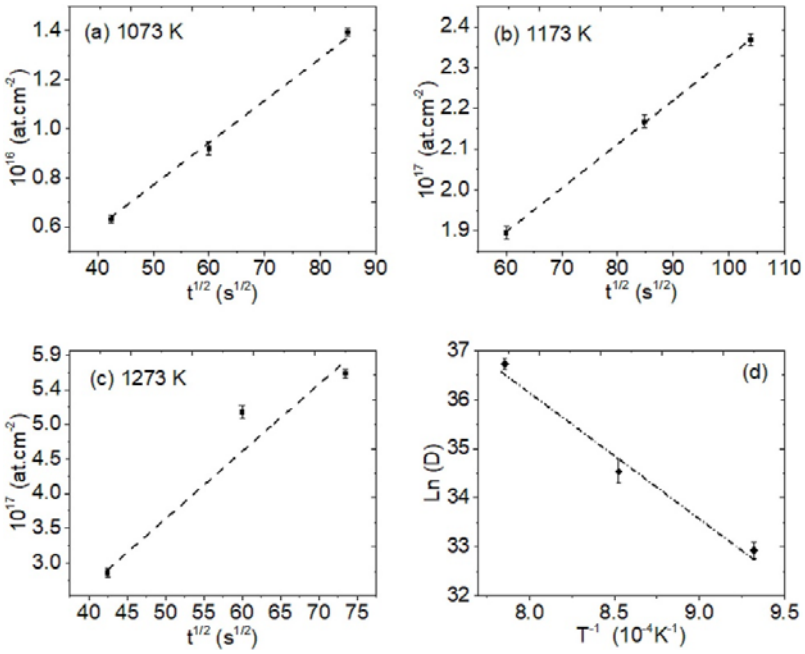

Fig. 6. Plots of intermixed layer thickness (x) vs. $t^{1/2}$ for temperatures at (a) 1073 (b) 1173 and (c) 1273 K. (d) Arrhenius plot for C diffusion in W.

The linear graphs obtained in these figures suggested that the growth kinetics of the intermixed layer was diffusion controlled. The slopes of these straight line graphs were the rate constants for their respective temperature and the values obtained are tabulated in Table 2.

Table 2. Temperature dependent diffusion parameters of the W/C couple.

Temp (*K*)	1/T (10^{-4} K^{-1})	k (at. cm^{-2} $\cdot$) $s^{-1/2}$	ln k	k_o ($m^2 \cdot s^{-1}$)	Q (eV)
1073	9.32	2.0×10^{14}	32.93	2.56×10^{-7}	2.23
1173	8.53	1.0×10^{15}	34.54		
1273	7.86	9.0×10^{15}	36.74		

To estimate the diffusion coefficient of the C in W, the following method was adopted. It is well known that the diffusion coefficient of the impurity atoms (C-atoms) can be obtained by the application of Arrhenius equation [34].

$$k = k_o \, exp\,(-Q/k_B T) \tag{2}$$

where k_o, Q, k_B and are the pre-exponential factor, activation energy, the Boltzmann constant and the absolute temperature, respectively. Consequently, the values of 1/ T and k were evaluated and plotted in accordance with the temperature dependent Arrhenius equation to obtain the graph shown in Fig. 6 (d). The activation energy was evaluated from Fig. 6(d) and the value obtained is presented in Table 2.

For diffusion in a cubic metallic structure such as tungsten, the pre-exponential factor k_o can be expressed as [35,36]:

$$k_o = \tfrac{1}{6} a^2 v \tag{3}$$

where a and v are the lattice constant and vibration frequency, respectively. The vibration frequency v_C of the interstitial carbon atom is given by Ref. [36]:

$$v_C = \sqrt{\frac{2Q}{ma^2}} \tag{4}$$

where is the mass of impurity atom. Using a mass of 1.9910^{-26} kg [31] for the carbon atom and a lattice constant of 3.17 X 10^{-10} m [18] for the BCC tungsten as well as the estimated activation energy of 2.23 eV, the vibration frequency is obtained as v_C = 1.89 10^{13} Hz. Substituting these values of a and v_C into Equation (3), the pre-exponential factor, k_o = 3.17 X 10^{-7} m^2s^{-1}. Hence, the general diffusion expression governing the interstitial diffusion of C in W is given by:

$$D = 3.17 \times 10^{-7} \left(m^2 \cdot s^{-1}\right) \exp\left(-\frac{2.23\ eV}{k_B T}\right) \tag{5}$$

where T is absolute temperature k_B is Boltzmann constant.

The value of activation energy of 2.23 eV obtained in this work is comparable to the range of activation energies (1.72–4.86 eV) [37], quoted for the diffusion of amorphous carbon in W_2C.

The possible reasons for the range of activation energies reported by Kharatyan et al. [37] could be due to differences in microstructure and defect volume of the diffusion couples used. Those materials might have been sourced from different manufacturers. In addition to these, differences in the range of temperatures adopted for diffusion study could also be a factor. A high activation energy has been attributed to difficulty in diffusion of carbon through the carbide phases [38,39]. The activation energy for C diffusion in W obtained in this study suggested the presence of carbide phase. But only the XRD technique can give a positive identification of the carbide phase formed.

3.3. XRD analysis

To complement the RBS results, all the samples were characterised by grazing incidence X-ray diffraction (GIXRD). This was meant to identify the phase composition of the diffusion couple and monitor any new phase formation as a result of the heat treatment. The diffractograms for the as deposited and annealed samples are shown in Fig. 7.

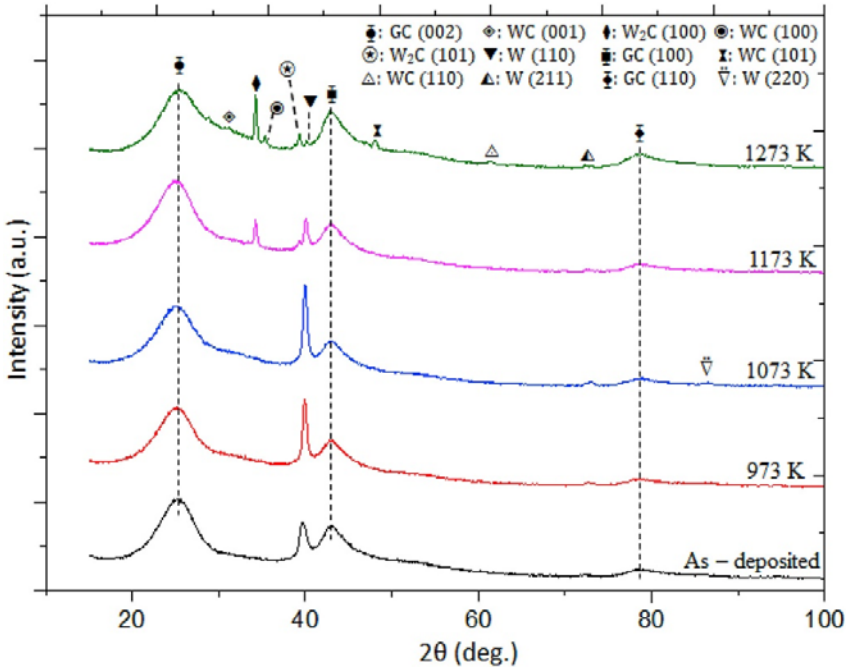

Fig. 7. XRD diffractograms of as-deposited and the annealed W/C samples. The glassy carbon peaks positions (GC) are 25.18, 43.10 and 79.07°; as-deposited W film peak positions are 39.73, 74.86 and 87.23°; W_2C peak positions are 34.19° and 39.29°; WC peak positions are 31.19, 35.32, 48.01 and 61.39°. Samples were vacuum annealed for 1 h at temperatures shown in the figure. All crystal planes are marked on the figure.

The phases were identified by comparing the peak position in the X-ray diffractograms with the peak position of the tungsten carbide standard tabulated in the ICDD-PDF-2 [40]. The comparison was supported by other papers [18,25,41]. The diffractogram of the as-deposited sample showed the presence of a strong diffraction peak at 2θ position of 39.73° and low intensity peaks at 74.86° and 87.23°, these peaks correspond to the (110), (211) and (220) orientation of W, respectively [40]. Also present was a strong broad peak at 25.18° and two other small broad peaks at 43.10° and 79.07°. These peaks correspond to the (002), (100) and (110) orientations of the graphitic domains in glassy carbon, respectively [15]. The broad nature of these peaks is characteristic of amorphous material due to scattered beams. This showed that

glassy carbon, indeed, contains a certain amount of amorphous material, often referred to in literature as nanocrystalline or paracrystalline material [42].

The absence of a carbide peak in the as-deposited sample showed that the XRD results were in good agreement with the RBS/RUMP simulated results, which showed no sign of atomic mixing or interaction at the interface. Similar diffraction peaks were observed in the sample annealed at 973 K, with the three additional features in the W (110) peak. This peak increased in intensity with reduced width, and a slight shift in the peak position to $2\theta = 39.93°$. The increase in the intensity of W peak upon annealing showed that the as-deposited W film was characterized by small grain size. The W film structure improved in its crystallinity upon annealing, hence the reduced width. The slight shift by 0.20° toward the higher 2θ angle can be attributed to residual stress relief due to annealing [43]. All the annealed samples experienced slight shifts in 2θ positions of the W(110) peak, with the sample annealed at 1173 K having the maximum shift of 0.33° from its initial peak position in the as-deposited sample (Table 3).

Table 3. Data extracted from the fitted diffraction patterns and the calculated crystallite size.

Temperature (K)	Phase identity	Peak position 2θ (Deg.)	FWHM (Deg.)	Crystallite size l_a (nm)
298.0	W(110)	39.7	0.91	9.8
973.0	W(110)	39.9	0.56	15.7
1173.0	W(110)	40.0	0.55	16.1
1273.0	W(110)	40.1	0.49	18.1

The sample annealed at 1073 K had the maximum intensity for W peak (110). This was due to the fact that at 1073 K, the W film had improved in its crystallinity and there was no carbide formed. The absence of a carbide phase in the diffraction pattern of this sample showed that the W/C couple was thermally stable at 1073 K. This was fairly in good agreement with the RBS results shown in Fig. 3. At 1073 K, the annealed temperature was not high enough to cause phase formation. The diffraction pattern for the sample annealed at 1173 K (Fig. 7) showed the presence of two additional peaks at 34.19° and 39.29°. These peaks were indexed as ditungsten carbide (W_2C) with orientation (100) and (101) planes, respectively. A similar observation was made by Wand and Jacob [25] who reported that the first phase which formed in tungsten-amorphous carbon multilayer films was W_2C at an annealing temperature of 1150 K.

Another feature associated with the diffraction pattern of the sample annealed at 1173 K was the drastic reduction in W (110) peak intensity. This is obviously reasonable since W was consumed to form W_2C. At the annealing temperature of 1273 K, the diffraction pattern indicated that the intensity of W_2C peak increased, while four new phases appeared at 2θ position of 31.19, 35.32, 48.01 and 61.39°. These peaks were indexed to tungsten monocarbide (WC) with (001), (100), (101) and (110) [40] crystal orientations, respectively. The formation of this additional carbide phase caused an almost complete depletion of the pure W peak. The W film had reacted completely with C to form carbides. Since more WC peaks appeared at 1273 K compared to the two peaks of W_2C which existed from 1173 K, it showed that further formation of W_2C was not favourable at this higher temperature. Luthin et al. [44] in their study on carbon film deposited on tungsten observed that W_2C was the first carbide phase to form and this phase later transformed to WC at a temperature of 1270 K. The formation of W-rich phase (W_2C) phase at a temperature of 1173 K could be attributed to the fact that, at this temperature, there was a low concentration of C in W after intermixing, hence favouring the formation of W_2C. At the higher

temperature (1273 K), more C had diffused into W. Consequently, there was large enough carbon concentration available such that the initially formed W_2C transformed to WC according to the reaction $W_2C + C \rightarrow 2WC$. Thus, it appears that the carbide phase formation sequence is a function of C concentration. Sequence of W_2C and WC formation observed in this study is in contrast to the sequence dictated by the W–C phase diagram [45], where WC exists before W_2C in the lower temperature regime. It is likely that high grain boundaries in the polycrystalline W film coupled with its less dense structure compared to the bulk W is responsible for this development.

To quantify the crystalline nature of the W film deposited, the diffractograms for all the samples were fitted with pseudo-Voigt function using the OriginLab program. This function is a convolution of both Lorentzian and Gaussian functions. Fig. 8 shows the fitted diffraction patterns for the as-deposited and annealed samples.

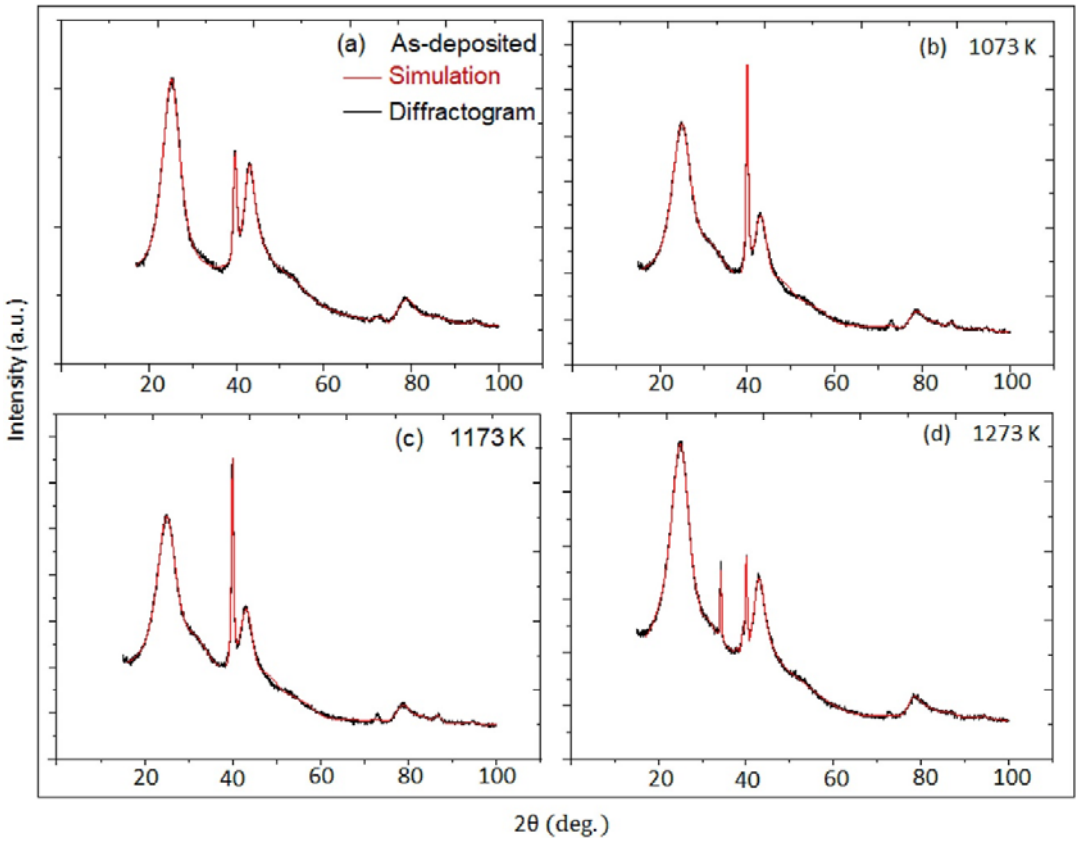

Fig. 8. Fitted XRD diffractions of (a) as deposited and the annealed samples at (b) 1073 K (c) 1173 K and (d) 1273 K.

From the fitted diffractograms above, the full width at half maximum (FWHM) and peak positions of W were determined. The values obtained are tabulated in Table 3.

The crystallite size (l_a) of the as-deposited W film and annealed samples were estimated with the aid of the Scherrer equation [46]:

$$l_a = \frac{k\lambda}{\beta \cos \theta} \quad (6)$$

where $\beta = \sqrt{B^2 - b^2}$, with being the FWHM of diffraction peak in radians and b is the instrumental broadening [46], λ = 1.5406 $\AA$ is the wavelength of Cu X-ray source used for XRD measurement, k is the Scherrer constant, taken as 0.94 while θ is the Bragg angle obtained from the peak positions. The instrumental broadening b is expressed by the relation [47,48]:

$$b = \tan^{-1}\left(\frac{W_R}{R_G}\right) + 2\left(\frac{\Delta\lambda}{\lambda}\right)\tan\ \theta \qquad (7)$$

where W_R is the receiving slit width (0.2 mm), R_G is the radius of goniometer (190 mm) and is $\angle\lambda$ resolution of the diffractometer 2 X 10^{-3}. Using Equations (6), (7)), the crystallite size l_a which is the average length of the graphitic lamellae within the glassy carbon [49], was estimated from the diffraction pattern of the as-deposited sample. The value of la was estimated as 2.57 nm, using the crystal orientation (100) [50] for the glassy carbon. This value is comparable with l_a = 3.10 nm obtained by Njoroge et al. [12], who worked on the same grade of glassy carbon, the Sigradur© G, using Raman spectroscopy analysis. The value for the average crystallite size obtained in this study supports the assertion that glassy carbon is a nanocrystalline material. The estimated average crystallite size for as-deposited W film is 9.77 nm, using the preferred crystal orientation (110). This showed that the W film deposited at room temperature was substantially composed of small grains. This finding is similar to results obtained by Hugon et al. [28], where the deposited W film had grain sizes varying from 13 to 50 nm depending on the W film thickness. In this study, the estimated crystallite size for the annealed samples increased steadily with annealing temperature (Table 3) up to 18.05 nm for the sample annealed at 1173 K.

The diffraction patterns show that there is no significant structural change to the glassy carbon. This is also supported by the fitting results, which show no sign of change in peak positions of the three prominent peaks indexed to glassy carbon. It shows that glassy carbon is thermally a stable material. The two non-destructive analytical techniques used in this study complemented each other well. XRD appears to be more sensitive to carbide phase formation than RBS. Although, both techniques showed the presence of the first carbide formed in the sample annealed at 1173 K, only the XRD technique positively identified this carbide phase. It was difficult to achieve that with RBS/RUMP technique. Good prediction for carbide phase with RBS occurred in the samples annealed at 1273 K.

4. Summary

The behaviour of W/C diffusion couples under heat treatment has been studied with RBS/RUMP and GIXRD. These two non-destructive analytical techniques have shown that the diffusion couples were thermally stable under heat treatment up to the annealing temperature of 1073 K, as no indication of a reaction was detected in this temperature regime. The RBS/RUMP results showed that interface mixing of atoms started at 1073 K and the intermixed layer growth increased progressively with annealing temperature and duration. The carbide phase W_2C was observed in the sample annealed at 1173 K for 60 min duration. It was observed that the amount of this carbide increased with the annealing temperature. At the annealing temperature of 1273 K, multiple peaks of WC appeared, as the dominant carbide phase. At this temperature, the W films had completely reacted with the C.

The diffusion analysis showed that the interaction between C and the W film was diffusion controlled. The estimated activation energy for C diffusion in W was 2.23 eV. The XRD results showed that glassy carbon was stable under the entire temperature regime used in this study. Its crystallite size was estimated as 2.57 nm, confirming the paracrystalline nature of glassy carbon. The W film deposited increased in its crystallinity upon annealing with increasing crystallite size.

The estimated crystallite size ranged from 9.77 nm in the as-deposited sample to 18.05 nm in the sample annealed at 1173 K for 1 h. Based on these results, the W/C couples are stable under heat treatment below 1073 K. In addition to the properties of glassy carbon and tungsten stated in the introduction section, the tungsten carbide formed contributes to the properties of the new system. Although, tungsten carbide is hard and tough against corrosion with good radiation shield, but hard materials are known to be brittle. This might bring about cracks development without warning. Except with appropriate alloying, the role tungsten carbide is questionable in a system where cracking is a serious concern. The radioactive decay heat in the nuclear waste decreases with storage time. The decay heat with temperature regime of 473 K might not contribute substantially to the degradation (if any) of this system. Therefore, it can be suggested that W/C couples are promising materials for fabrication of long term nuclear waste storage devices.

Declaration of competing interest

We hereby declare that there is no competing interest that can influence the outcome of this study.

Acknowledgement

Author IAJ sincerely appreciates Mr T. Ntsoane and Dr A. Venter of NECSA for their help with the XRD measurement.

References

[1] M.I. Ojovan, W.E. Lee, Glassy wasteforms for nuclear waste immobilization, Metall. Mater. Trans. 42 (2011) 837–851.
[2] O. Chopra, D. Diercks, D. Ma, V. Shah, S.-W. Tam, R. Fabian, Y. Liu, M. Nutt, Managing aging effects on used fuel dry cask for very long-term storage, in: ASME 2011 14th International Conference on Environmental Remediation and Radioactive Waste Management, American Society of Mechanical Engineers, pp. 715-722.
[3] D.B. Rigby, Evaluation of the Technical Basis for Extended Dry Storage and Transportation of Used Nuclear Fuel: Executive Summary, US Nuclear Waste Technical Review Board, 2010.
[4] Y.Y. Liu, D.R. Diercks, O.K. Chopra, M. Nutt, Managing Aging Effects on Dry Cask Storage Systems for Extended Long-Term Storage and Transportation of Used Fuel, Technical Report, Argonne National Lab.(ANL), Argonne, IL (United States), 2015.
[5] M. Liu, V.I. Artyukhov, H. Lee, F. Xu, B.I. Yakobson, Carbyne from first principles: chain of C atoms, a nanorod or a nanorope, ACS Nano 7 (2013) 10075–10082.
[6] A. Ferrari, J. Robertson, Resonant Raman spectroscopy of disordered, amorphous, and diamond-like carbon, Phys. Rev. B 64 (2001) 1–13.
[7] M. Hu, J. He, Z. Zhao, T.A. Strobel, W. Hu, D. Yu, H. Sun, L. Liu, Z. Li, M. Ma, et al., Compressed glassy carbon: an ultrastrong and elastic interpenetrating graphene network, Science advances 3 (2017) 160–213.
[8] D. McCulloch, S. Prawer, A. Hoffman, Structural investigation of xenon ion beam irradiated glassy carbon, Phys. Rev. B 50 (1994) 5905–5910.
[9] A. Craievich, On the structure of glassy carbon, Mater. Res. Bull. 11 (1976) 1249–1255.
[10] M.I. Nathan, J.E. Smith Jr., K. Tu, Raman spectra of glassy carbon, J. Appl. Phys. 45 (1974), 2370-2370.
[11] T.T. Hlatshwayo, L. Sebitla, E.G. Njoroge, M. Mlambo, J.B. Malherbe, Annealing effects on the migration of ion-implanted cadmium in glassy carbon, Nucl. Instrum. Methods Phys. Res.

Sect. B Beam Interact. Mater. Atoms 395 (2017) 34–38.
[12] E.G. Njoroge, L. Sebitla, C. Theron, M. Mlambo, T.T. Hlatshwayo, O. S. Odutemowo, V. Skuratov, E. Wendler, J.B. Malherbe, Structural modification of indium implanted glassy carbon by thermal annealing and SHI irradiation, Vacuum 144 (2017) 63–71.
[13] P.K. Chu, L. Li, Characterization of amorphous and nanocrystalline carbon films, Mater. Chem. Phys. 96 (2006) 253–277.
[14] T. Noda, M. Inagaki, S. Yamada, A comment on the structure of glassy carbon, Bull. Chem. Soc. Jpn. 41 (1968) 3023–3024.
[15] S. Bukalov, L. Leites, A. Sorokin, A. Kotosonov, Structural changes in industrial glassy carbon as a function of heat treatment temperature according to Raman spectroscopy and X-ray diffraction data, Nanosystems: Physics, Chemistry, Mathematics 5 (2014) 186–191.
[16] A. De Luca, A. Portavoce, M. Texier, C. Grosjean, N. Burle, V. Oison, B. Pichaud, Tungsten diffusion in silicon, J. Appl. Phys. 115 (2014) 135–141.
[17] V. Philipps, Tungsten as material for plasma-facing components in fusion devices, J. Nucl. Mater. 415 (2011) S2–S9.
[18] E. Lassner, W.D. Schubert, Tungsten: Properties, Chemistry, Technology of the Element, Alloys, and Chemical Compounds, Kluwer Academic/Plenum Publishers, New York, 1999.
[19] V. Lavrentiev, J. Vacik, H. Naramoto, Structural phenomena in glassy carbon induced by cobalt ion implantation, Appl. Phys. A 92 (2008) 673–680.
[20] D. Langa, N. Van Der Berg, E. Friedland, J.B. Malherbe, A. Botha, P. Chakraborty, E. Wendler, W. Wesch, Heat treatment of glassy carbon implanted with cesium at room and high temperatures, Nucl. Instrum. Methods Phys. Res. Sect. B Beam Interact. Mater. Atoms 273 (2012) 68–71.
[21] Hochtemperatur-werkstoffe GmbH, Germany, properties of glassy carbon. http://htw-germany.com/technology.php5?lang¼en&nav0¼2& nav1¼16. (Accessed 28 October 2019).
[22] Advanced Energy, USA, MDX series of magnetrons. http://htw-germany.com/technology.php5?lang¼en&nav0¼2&nav1¼16. (Accessed 3 January 2020).
[23] A.J. Innocent, T.T. Hlatshwayo, E.G. Njoroge, J.B. Malherbe, Interface interaction of tungsten film deposited on glassy carbon under vacuum annealing, Vacuum 148 (2018) 113–116.
[24] M. Birkholz, Thin Film Analysis by X-Ray Scattering, John Wiley & Sons, New York, 2006.
[25] P. Wang, W. Jacob, Deuterium diffusion and retention in a tungsten-carbon multilayer system, Nucl. Instrum. Methods Phys. Res. Sect. B Beam Interact. Mater. Atoms 329 (2014) 6–13.
[26] N. Barradas, Double scattering in grazing angle Rutherford backscattering spectra, Nucl. Instrum. Methods Phys. Res. Sect. B Beam Interact. Mater. Atoms 225 (2004) 318–330.
[27] H. Jehn, G. Bar, E. Best, E. Koch, Reactions with carbon, in: W Tungsten: Supplement Volume A 5B Metal, Chemical Reactions with Nonmetals Nitrogen to Arsenic, Springer, Berlin, 1993, pp. 131–154.
[28] M.C. Hugon, C. Arena, B. Agius, M. Froment, F. Varniere, C. Vignaud, Structure and properties of rf magnetron sputtered W films, Microsc. Microanal. Microst. 1 (1990) 175–187.
[29] G. Lamble, S. Heald, D. Sayers, E. Ziegler, P. Viccaro, Glancing angle EXAFS investigations of the effects of annealing on WC multilayer composition, Phys. B Condens. Matter 158 (1989) 672–673.
[30] C. Wei-Kan, J. Mayer, M. Nicolet, Backscattering Spectrometry, Academic Press, New York, 1978.
[31] W.D. Callister, D.G. Rethwisch, Materials Science and Engineering: an Introduction, vol 7, John wiley & sons, New York, 2007.
[32] K. Bhanumurthy, R. Schmid-Fetzer, Interface reactions between silicon carbide and metals (Ni, Cr, Pd, Zr), Compos. Appl. Sci. Manuf. 32 (2001) 569–574.

[33] F. Goesmann, R. Schmid-Fetzer, Metals on 6H-SiC: contact formation from the materials science point of view, Mater. Sci. Eng., B 46 (1997) 357–362.
[34] K.J. Laidler, The development of the Arrhenius equation, J. Chem. Educ. 61 (1984) 494–502.
[35] Y.L. Liu, H.B. Zhou, S. Jin, Y. Zhang, G.H. Lu, Dissolution and diffusion properties of carbon in tungsten, J. Phys. Condens. Matter 22 (2010) 445–504.
[36] C. Wert, C. Zener, Interstitial atomic diffusion coefficients, Phys. Rev. 76 (1949) 1169–1175.
[37] S. Kharatyan, H. Chatilyan, L. Arakelyan, Kinetics of tungsten carbidization under non-isothermal conditions, Mater. Res. Bull. 43 (2008) 897–906.
[38] M.R. Andrews, Diffusion of carbon through tungsten and tungsten carbide, J. Phys. Chem. 29 (1925) 462–472.
[39] K. Schmid, J. Roth, Concentration dependent diffusion of carbon in tungsten, J. Nucl. Mater. 302 (2002) 96–103.
[40] H.F. McMurdie, M.C. Morris, E.H. Evans, B. Paretzkin, W. Wong-Ng, L. Ettlinger, C. R. Hubbard, Standard X-Ray Diffraction Powder Patterns from the JCPDS Research Associateship, Cambridge University Press, 1986.
[41] M.B. Zellner, J.G. Chen, Synthesis, characterization and surface reactivity of tungsten carbide (WC) PVD films, Surf. Sci. 569 (2004) 89–98.
[42] K. Jurkiewicz, S. Duber, A. Burian, Paracrystalline structure of glasslike carbons, Int. J. Appl. Glass Sci. 7 (2016) 355–363.
[43] Y. Yang, S. Zhao, J. Gong, X. Jiang, C. Sun, Effect of heat treatment on the microstructure and residual stresses in (Ti, Al) N films, J. Mater. Sci. Technol. 27 (2011) 385–392.
[44] J. Luthin, C. Linsmeier, Influence of oxygen on the carbide formation on tungsten, J. Nucl. Mater. 290 (2001) 121–125.
[45] A. Kurlov, A. Gusev, Tungsten carbides and WC phase diagram, Inorg. Mater. 42 (2006) 121–127.
[46] B.D. Cullity, S.R. Stock, Elements of X-Ray Diffraction, Addison-Wesley Publishing company Inc, Massachusetts, 1956.
[47] B. Mallick, X-ray diffraction analysis of polymeric solid using Bragg Brentano geometry, Int. J. Mater. Chem. Phys 1 (2015) 265–270.
[48] T. Ida, K. Kimura, Flat-specimen effect as a convolution in powder diffractometry with Bragg-Brentano geometry, J. Appl. Crystallogr. 32 (1999) 634–640.
[49] P.J. Harris, Structure of non-graphitising carbons, Int. Mater. Rev. 42 (1997) 206–218.
[50] Y.J. Lee, The second order Raman spectroscopy in carbon crystallinity, J. Nucl. Mater. 325 (2004) 174–179.